^{18}O+^{110}Pd: Measurements and realistic coupled-channel analysis in a transitional region

D. Pereira, E. S. Rossi, Jr., G. P. A. Nobre, L. C. Chamon, C. P. Silva, L. R. Gasques, M. A. G. Alvarez, R. V. Ribas, J. R. B. Oliveira, N. H. Medina, M. N. Rao, E. W. Cybulska, W. A. Seale, and N. Carlin
Departamento de Física Nuclear, Instituto de Física da Universidade de São Paulo, São Paulo, SP, Brazil, CP 66318, 05315-970

P. R. S. Gomes, J. Lubian, and R. M. Anjos
Instituto de Física, Universidade Federal Fluminense, Niterói, RJ, Brazil, 24210-340
(Received 31 May 2006; published 28 September 2006)

The inelastic, two-neutron and α transfer and quasielastic cross sections for the ^{18}O+^{110}Pd system have been measured in the near barrier region (40 MeV $\leqslant E_{\rm lab} \leqslant$ 58 MeV). The experiments were performed in the São Paulo Pelletron laboratory. Coupled-channel analysis of the experimental data was performed using the São Paulo potential as a microscopic bare interaction. In the calculations, low-lying inelastic excitations, one- and two-neutron and α transfers to the target were considered as the main couplings, with no extra surface absorption. The agreement between the theoretical results and the experimental data is good. The role played by the coupled channels is very different in comparison with similar data analyses for the closed-shell region around ^{58}Ni.

DOI: 10.1103/PhysRevC.74.034608 PACS number(s): 25.70.Bc, 25.70.Hi, 24.10.Eq

I. INTRODUCTION

The São Paulo potential (SPP) microscopic bare interaction [1–3] provides a reliable starting point for the analysis of nuclear reaction data. It is theoretically founded on the Pauli nonlocality, which arises from quantum exchange effects. It has been experimentally tested in a wide variety of mass and energy regions in combination with different theoretical approaches [4–12].

The SPP contains no adjustable parameter and, combined with coupled-channel (CC) calculations, provides a powerful tool for predicting cross sections for quite different systems and energies. This procedure has been applied successfully in the description of elastic scattering, peripheral reaction channels, and fusion for several near closed-shell systems (particularly around O+Ni) over a wide energy range. It has been possible, by introduction of the low-lying channel couplings, to obtain a good description of the data with no imaginary optical potential at the surface region.

In the present work, with the aim to extend the successful SPP/CC approach to a well-known transitional region ($A \approx 100$), we have measured the inelastic, two-neutron and α-transfer cross sections by γ-particle coincidence for the ^{18}O+^{110}Pd system in the near-barrier region (40 MeV $\leqslant E_{\rm lab} \leqslant$ 58 MeV). The $l = 0$ barrier (V_B^0) value is 46.6 MeV in the laboratory system. The target (^{110}Pd) is a neutron-rich stable isotope for which previous experimental data analysis on elastic and inelastic scattering of α particles is available [13]. The γ-particle coincidence measurements were essential for the separation of the low-lying states of the inelastic and transfer channels. The experimental data set was complemented by quasielastic (elastic, inelastic, and few-nucleon transfer) differential cross sections measured by particle detection methods in the same energy region.

The main objectives of this experiment were to learn: (i) whether it is possible to obtain a good description of a nuclear reaction with strong channel couplings with the SPP bare potential; (ii) the relative importance of different channel couplings in comparison with the nearly spherical Ni region; (iii) which other dynamical polarization effects might be important in the CC analysis (e.g., dissipative and deep inelastic mechanisms).

The article is organized as follows: Sec. II presents the experimental details, in Sec. III the experimental results are compared to the CC theoretical calculations, Sec. IV discusses fusion hindrance and enhancement, and in Sec. V, the summary of the work and main conclusions are presented.

II. EXPERIMENTAL SETUP AND PROCEDURES

A. γ-particle coincidence measurements

The time coincidences of γ rays and beamlike particles were measured for the ^{18}O+^{110}Pd reaction at 10 different beam energies between 40 and 58 MeV. The ^{18}O beam was provided by the 8-MV Pelletron Tandem accelerator of the University of São Paulo (IFUSP-DFN). The target used was a self-supported 1-mg/cm^2-thick enriched ^{110}Pd (>97%) foil. The beam-energy loss through the target is around 3 MeV. The beamlike particles were detected by a Si surface barrier annular detector covering the angular range between 158.6° and 173.2° relative to the beam direction ($\Delta\Omega \approx 0.4$ sr). The γ rays were detected by two hyperpure germanium detectors (ORTEC, nominally 20% photopeak efficiency relative to a $3 \times 3''$ NaI(Tl) scintillator) disposed at 71° and 120° relative to the beam direction. A Si surface barrier detector monitor was placed at 45° to the beam direction for normalization. The relative γ-ray efficiencies were determined with a ^{152}Eu radioactive source.

Six spectra were accumulated for each run, corresponding to the energies of each of the four detectors and the coincidence time spectra between the γ-ray detectors and the annular detector. Gates were set at the prompt peak of the time spectra and at the beamlike particle energy region of the annular detector spectrum to form the coincidence γ-ray spectra.

Chance events were subtracted off-line by gating in the random coincidence time region.

The relative normalization between different runs was obtained by multiplying the number of counts of the monitor detector by the square of the corresponding average beam energy on the target. Assuming pure Rutherford scattering at this fixed angle, this number should be proportional to the integrated beam intensity. The error made in this assumption is estimated to be less than 5% up to the highest beam energy used, according to Coulomb excitation calculations. However, because the target is quite thick, causing energy and angular straggling, a wide gate has to be set in the monitor spectrum and therefore some contamination from the degraded beam scattered on slits, annular detector collimator, and on lower-Z target contaminants could also be counted. These problems are strongest at the lowest energy and reduce rapidly as the energy increases. This results in underestimated reaction cross sections relative to the higher energies. We estimate the error in the relative normalization between the lowest and highest energy measured to be no more than 15%. This is a systematic error that could not be evaluated very precisely and, for this reason, has not been included in the uncertainties presented in the figures.

The coulomb excitation code GOSIA [14] was used to fit the observed yields of the $2^+ \rightarrow 0^+$, $4^+ \rightarrow 2^+$, $2_2^+ \rightarrow 2^+$, and $2_2^+ \rightarrow 0^+$ transitions in ^{110}Pd at the safe energies (for which the nuclear interaction is negligible) of 40, 44, and 46 MeV. The transition and intrinsic reduced matrix elements obtained were consistent with the adopted values from the literature. The angular distribution parameters, necessary for correcting the yields at the fixed γ-detector angles, were calculated by the code considering upper-level feeding, the geometry and absorbers of the detectors, the integration over the beam-energy variation through the target, and the deorientation due to the hyperfine interaction of the recoil in vacuum. The vacuum deorientation strongly attenuates the γ-decay angular anisotropy. With the detector angles chosen, the maximum error that would result by assuming isotropic distributions was calculated to be less than 5% for all the pure Coulomb excitation cases. For this reason, the same angular distribution correction for each state was applied for the higher energies and for the corresponding states of the transfer reaction channels (^{112}Pd and ^{114}Cd). Figure 1 presents the backscattered particle-gated γ spectra at two different beam energies.

The final excitation cross sections (integrated in the angular range of the annular detector) were obtained by normalizing the data point of the 364-keV transition of ^{110}Pd ($2^+ \rightarrow 0^+$) at the average beam energy of $\langle E_{\rm lab} \rangle = 42.5$ MeV to the theoretical result of the full coupled-channels calculation at the same energy. At that energy the nuclear interaction is negligible and the reliable Coulomb excitation cross-section is recovered. In this manner, cross sections for the following states were obtained: 2_1^+, 2_2^+, and 4_1^+ of ^{110}Pd; 2_1^+ and 4_1^+ of ^{112}Pd; and 2_1^+ of ^{114}Cd. For the $1n$ transfer channel (^{111}Pd) only rough estimates for some of the low-lying states were obtained due to the weakness and fragmentation of the transitions and to the large Compton background in the energy region of the peaks (Fig. 1).

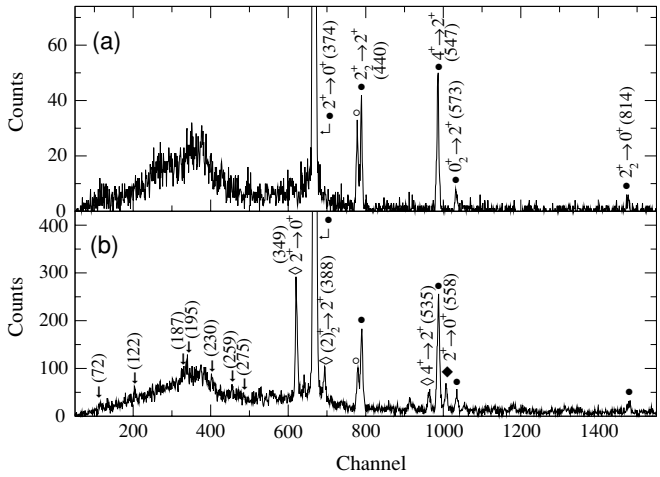

FIG. 1. γ-ray spectra gated by backscattered beamlike particles at the average beam energy of (a) $\langle E_{\rm lab} \rangle = 42.5$ MeV and (b) $\langle E_{\rm lab} \rangle = 51.1$ MeV. The numbers in parentheses are the peak energies in keV. The closed circles are peaks from inelastic scattering (^{110}Pd), open diamonds from two-neutron transfer (^{112}Pd), closed diamond from α-particle transfer (^{114}Cd), and downward arrows in the 70- to 280-keV region indicate peak positions expected for one neutron transfer (^{111}Pd), barely seen. The bump in both spectra observed in that same energy region comes essentially from Compton scattering of the large 374 keV ^{110}Pd $2^+ \rightarrow 0^+$ inelastic peak. The open circle indicates the $2^+ \rightarrow 0^+$ inelastic peak (434 keV) from the main isotopic contamination of the target: ^{108}Pd (∼2.5%).

B. Quasielastic measurements with particle detection

The angular distributions were measured with the ^{18}O beam from the São Paulo 8UD Pelletron tandem accelerator at 42.5, 46.0, 50.5, 51.3, 52.5, 53.5, and 55 MeV, in the $40^\circ \leqslant \theta_{\rm lab} \leqslant 170^\circ$ angular range in 5° steps. The detection system consists of a set of nine surface barrier detectors spaced 5° apart. In front of each detector there was a set of three collimators to avoid slit-scattered particles from reaching the detectors. The solid angle and the angular aperture for each detector and the target were 4.0×10^{-4}sr and 0.6°, respectively. The thickness of the enriched (>97%) ^{110}Pd target was about 100 μg/cm^2, evaporated onto a carbon foil (10 μg/cm^2). A layer of gold (20 μg/cm^2) was evaporated on the target for normalization. The energy resolution was about 350 keV, mainly due to the energy loss through the target. In Fig. 2 a typical energy spectrum is shown, illustrating the two partially separated groups (together denominated quasielastic), one relative to elastic and the other to inelastic and transfer processes.

III. EXPERIMENTAL RESULTS AND CC DATA ANALYSIS

A. Experimental results

In Figs. 3, 4, and 5 we present the excitation functions for the integrated ($158.6^\circ < \theta_{\rm lab} < 173.2^\circ$) cross section values using the γ-particle coincidence method (Sec. II), for the

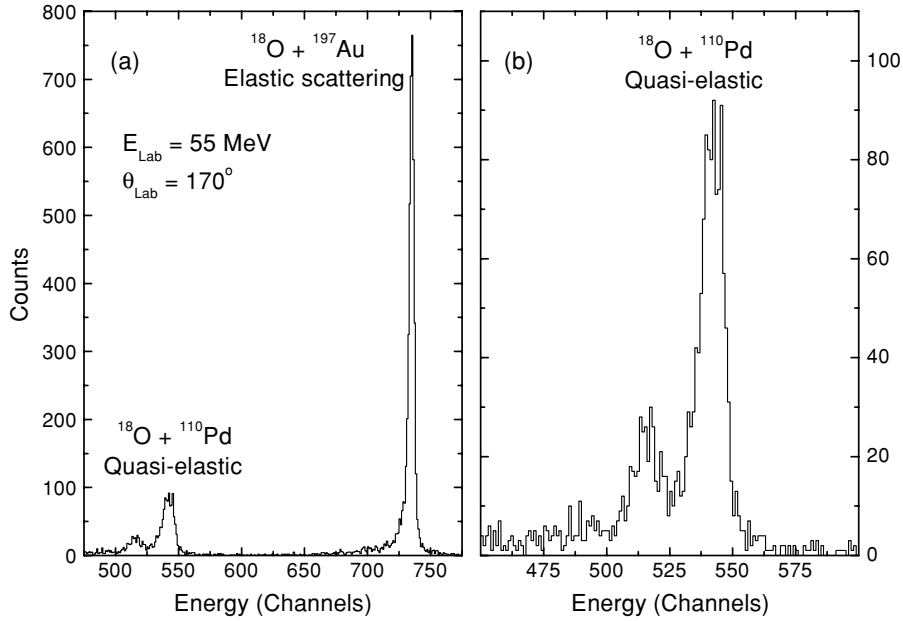

FIG. 2. (a) Energy spectrum at $E_{\rm lab} = 55$ MeV and $\theta_{\rm lab} = 170^\circ$. The peaks correspond to the elastic and quasielastic scattering processes for the systems as indicated. (b) Expansion of (a) in the region of the quasielastic peaks (dominated by the elastic and 2_1^+ inelastic excitation peaks) for the ^{18}O+^{110}Pd system.

inelastic excitations (inel) of ^{110}Pd ($2_1^+, 2_2^+$, and 4_1^+states), the two-neutron ($2n$) transfer reactions ($2_1^+$and 4_1^+ states of ^{112}Pd), and the α transfer reaction (2_1^+ state of ^{114}Cd). As shown in Fig. 3, the cross-section measurements cover an energy interval between -7 and $+9$ MeV relative to the $l = 0$ barrier value: $V_B^0 = 46.6$ MeV. The experimental cross-section detection limit using the technique and procedures described in Sec. II is about 10 μb. The $2n$ and α transfer reaction cross sections are presented in Figs. 4 and 5, respectively. The experimental uncertainties indicated in the figures are from peak fit adjustment and statistical origins. The uncertainty in the average energy due to the straggling of the beam through the 1-mg/cm^2 Pd target is around 1% and has been incorporated in the theoretical calculation (Sec. III B).

The quasielastic angular distributions at $E_{\rm lab} = 50.5, 51.5, 52.5, 53.5$, and 55 MeV are shown in Fig. 6. For the energies $E_{\rm lab} \leqslant 52.5$ MeV the experimental data points are restricted to angles greater than $\theta_{\rm cm} = 110^\circ$ because at these energies and for forward angles, the inelastic and few-nucleon transfer events are somewhat contaminated by degraded beam-scattered particles. The final differential cross section values were obtained by data normalization at the backward-scattering angle $\theta \geqslant 100^\circ$ at the energies of 42.5 and 46 MeV for each detector. As mentioned before, at these energies only Coulomb effects are expected (Sec. II) in the scattering angle region investigated. Using this procedure we estimated the uncertainties in the absolute differential cross section values to be no more than 10%.

B. Coupled-channel data analysis for the ^{18}O+^{110}Pd system

For the CC data analysis we have used the microscopic Pauli nonlocal potential known as the São Paulo potential. Within this model the nuclear potential is

$$V_N(R) = V_F(R) e^{-4v^2(R)/c^2}, \qquad (1)$$

where $v(R)$ is the local relative velocity between the colliding nuclei and $V_F(R)$ is the double-folding potential. For a heavy system such as ^{18}O+^{110}Pd, at near-barrier energies and interacting distances around the barrier radius, the effect of the velocity dependence in Eq. (1) is quite small (about 1%–2%). However, with a significant overlap of the colliding nuclei,

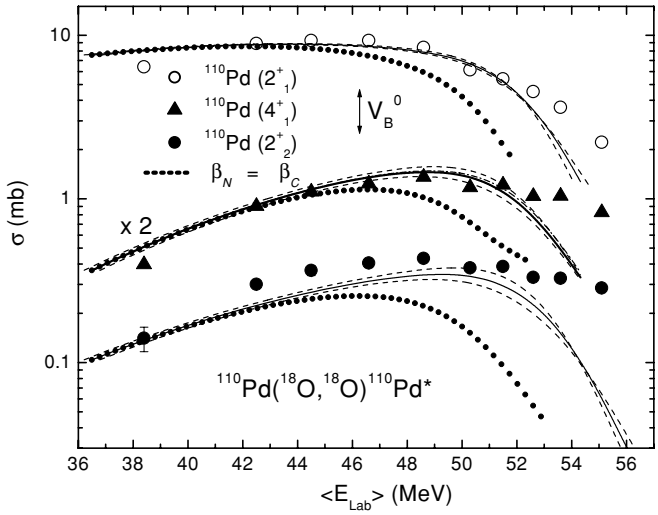

FIG. 3. Excitation functions for the inelastic integrated cross-sections ($158.6^\circ \leqslant \theta \leqslant 173.2^\circ$) measured with the γ-particle coincidence method for the $2_1^+, 2_2^+$, and 4_1^+ states in ^{110}Pd at $E^* = 374$, 814, and 921 keV, respectively. Most error bars are slightly smaller than the symbol sizes. The solid lines correspond to the full CC calculation results (inel + $2n + \alpha + 1n$). The dashed lines indicate upper and lower limits of the full CC results due to the variation of the deformation parameters β_N (in the range indicated in Table I) and to the beam energy straggling through the target. The effect of the $2n$, α, and $1n$ couplings is small, and the corresponding partial results lie within the dashed curves. The thick dot curves represent the full CC results for $\beta_N = \beta_C$.

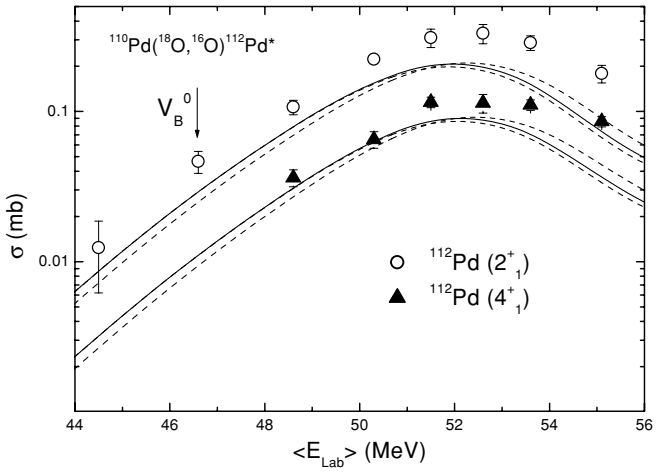

FIG. 4. Excitation functions for the $2n$ transfer cross sections ($158.6^\circ \leqslant \theta \leqslant 173.2^\circ$) measured with the γ-particle coincidence method for the 2_1^+(open circles) and 4_1^+(closed triangles) states in ^{112}Pd at $E^* = 434$ and 1048 keV, respectively. The solid lines correspond to the full CC (inel $+2n + \alpha + 1n$) calculation. The dashed lines indicate upper and lower limits of the full CC results considering variation in the deformation parameter β_N values (Table I) and in the beam energy straggling through the target.

it gives rise to dynamical saturation effects in the nuclear potential (equivalent to a repulsive force). In the model these effects are due to the exchange of nucleons between the target and projectile and are calculated in a first-order approach ($kb \ll 1$), where b is the corresponding nonlocality range. The ground-state density involved in the folding V_F potential was determined experimentally for ^{18}O [15] and based on Hartree-Fock-Bogoliubov (HFB) calculations as reported in Ref. [3] for ^{110}Pd. For the sake of illustration, the equivalent Woods-Saxon (WS) shape potential that simulates the São Paulo bare interaction has the following parameters: $V_0 = 200$ MeV, $r_0 = 1.06$ fm, and $a = 0.74$ fm at $E_{\rm lab} = 46$ MeV. The ^{18}O density was obtained experimentally through the subbarrier quasielastic data analysis for the ^{18}O+^{58}Ni system as described in detail in Ref. [16]. The large diffuseness parameter ($a = 0.74$ fm), as compared with other systems with ^{16}O as the projectile ($a \approx 0.6$ fm), is due to the effect of the two extra neutrons on the ^{18}O density [15], relative to that for the doubly magic nucleus. The CC calculations were performed with the program FRESCO [17]. Some other general details concerning the calculations are similar to those reported in Ref. [16] for the ^{18}O + ^{58}Ni system, and will not be presented in this article.

The channels included in the present CC calculation are those expected to have significant couplings to the elastic channel, based on similar studies for the ^{18}O+^{58}Ni system. Table I lists the inelastic channel excitations, and Table II the transfer reactions included in the calculation. The inelastic (^{110}Pd) states were treated as collective (vibrational), as suggested by earlier (α, α') studies [13], and their form factors were chosen to be the derivatives of the monopole potential, with deformation lengths (δ) listed in Table I. The Coulomb deformation parameters β_C for the inelastic excitations (see Table I) were obtained from the $B(E2)$

TABLE I. Deformation parameters used in the present CC calculation for the ^{18}O + ^{110}P system. The upper and lower limits in the β_N/β_C ratio corresponds to the variation interval shown in Fig. 3 (dashed lines) for illustration of the respective sensitivity of the calculation. See text for details.

Nucleus	Transition	δ_C(fm)	β_C	β_N/β_C	δ_N (fm)
^{110}Pd	$0^+_{gs} \rightarrow 2^+_1$	1.62	0.30	0.35^{+10}_{-15}	0.57
^{110}Pd	$2^+_1 \rightarrow 2^+_2$	0.72	0.14	0.35^{+10}_{-15}	0.25
^{110}Pd	$2^+_1 \rightarrow 4^+_1$	1.26	0.24	0.75^{+10}_{-10}	0.95
^{110}Pd	$2^+_1 \rightarrow 0^+_2$	0.82	0.15	0.35^{+10}_{-15}	0.29
^{110}Pd	$0^+_{gs} \rightarrow 2^+_2$	0.067	0.035	0.35^{+10}_{-15}	0.024
^{18}O	$0^+_{gs} \rightarrow 2^+_1$	1.26	0.49	1.00	1.26

values reported in the literature and procedures described in Ref. [18]. The corresponding β_N nuclear potential deformation parameters might be expected to be similar to β_C, as verified for the nearly closed-shell O+Ni systems. However, significant discrepancies between these parameters have been reported for transitional and deformed regions (e.g., Ref. [13]). Based on this fact, in the present calculation, β_N were assumed to be variable parameters (Table I). The optical potential in the elastic and inelastic channels was assumed to be identical.

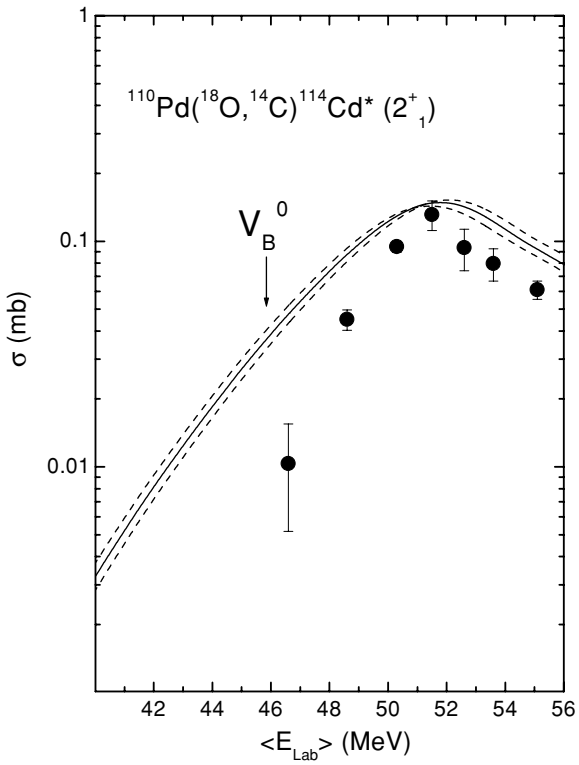

FIG. 5. Excitation functions for the α-transfer cross section ($158.6^\circ \leqslant \theta \leqslant 173.2^\circ$) measured with the γ-particle coincidence method for the 2_1^+ state in ^{114}Cd at $E^* = 558$ keV. The solid line is the full CC curve. The region between dashed lines correspond to the deformation parameter variation presented in Table I and the uncertainty due to energy straggling.

TABLE II. The N, L, S, and J quantum numbers, relative spectroscopic amplitudes (A) and factors (c^2s) included in the present CC calculation for the various transfer reactions.

Reaction	N	L	S	J	$A = \sqrt{c^2s}$	c^2s
(^{18}O gs, ^{16}O gs)	2	0	0	0	0.48	0.23
(^{110}Pd gs, ^{112}Pd gs)	4	0	0	0	0.48	0.23
(^{110}Pd gs, ^{112}Pd 2_1^+)	3	2	0	2	0.48	0.231[a]
(^{110}Pd gs, ^{112}Pd 4_1^+)	2	4	0	4	0.32	0.11[a]
(^{110}Pd gs, ^{112}Pd 0_2^+)	4	0	0	0	0.32	0.11
(^{110}Pd gs, ^{112}Pd 2_2^+)	3	2	0	2	0.32	0.11
(^{18}O gs, ^{14}C gs)	1	0	0	0	2.66	7.1
(^{110}Pd gs, ^{114}Cd gs)	3	0	0	0	2.66	7.1
(^{110}Pd gs, ^{114}Cd 2_1^+)	2	2	0	2	2.66	7.1
(^{18}O gs, ^{17}O gs)	1	2	1/2	5/2	1.00	1.000
(^{110}Pd gs, ^{111}Pd $\frac{5}{2}^+_1$)	2	2	1/2	5/2	0.36	0.132[b]
(^{110}Pd gs, ^{111}Pd $\frac{1}{2}^+_1$)	3	0	1/2	1/2	0.60	0.36[b]
(^{110}Pd gs, ^{111}Pd $\frac{1}{2}^+_2$)	3	0	1/2	1/2	0.37	0.14[b]
(^{110}Pd gs, ^{111}Pd $\frac{3}{2}^+_1$)	2	2	1/2	3/2	0.62	0.38[b]

[a]Experimentally determined in this work.
[b]From (d, p) reaction.

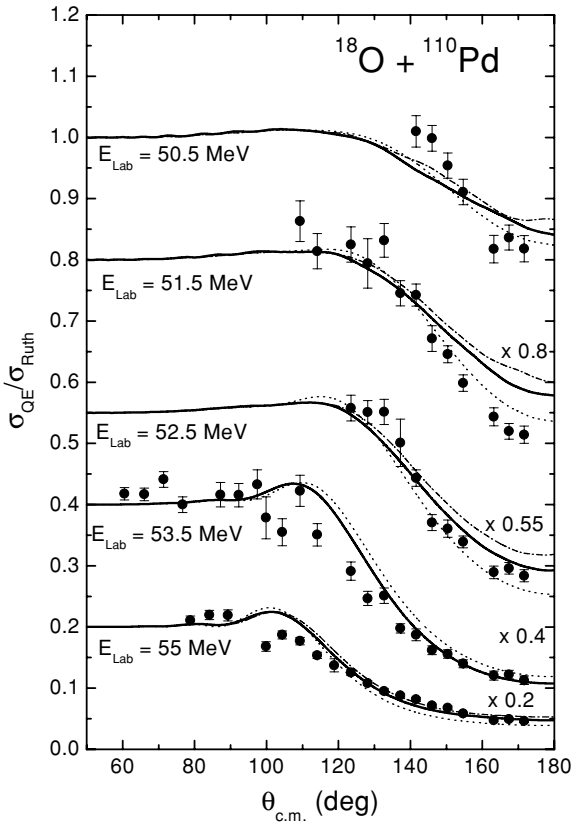

FIG. 6. Experimental quasielastic differential relative cross section values for the ^{18}O+^{110}P system at the bombarding energies of $E_{\rm lab} = 50.5$, 51.5, 52.5, 53.5, and 55 MeV. The line conventions are: full CC = inel + $2n + \alpha + 1n$ (solid); inel only and inel + $2n$ (these two nearly superposed, dot); inel + $2n + \alpha$ (dash-dot). The effect of the uncertainties in β_N parameters is negligible (about 1% for $\theta_{\rm cm} > 100^\circ$) in this inclusive data.

The spectroscopic factors for the one-neutron transfer reaction for the ^{111}Pd states of $I^\pi = \frac{5}{2}^+_1$(gs), $\frac{1}{2}^+_1$ ($E^* = 72$ keV), $\frac{1}{2}^+_2$ ($E^* = 192$ keV), and $\frac{3}{2}^+_1$ ($E^* = 195$ keV), as shown in Table II, were those from light ion reactions [19] assuming the same normalization, as discussed in Ref. [20], for the (^{18}O, ^{17}O) and (d, p) reactions. This procedure was necessary due to the difficulties to obtain acceptable precise cross sections for the ^{110}Pd(^{18}O,^{17}O)^{111}Pd reaction at near barrier energies by the γ-particle method (see Sec. II). The order of magnitude of the excited states cross sections calculated ($\leqslant$0.3 mb) is consistent, considering the fragmentation of the decay, with the low number of counts in the corresponding peaks of Fig. 1.

For the two-neutron (^{18}O,^{16}O) and α- (^{18}O,^{14}C) transfer reactions we have assumed $S = 0$ cluster form factors. No sequential transfers of particles or clusters of particles were considered in our calculations as they would give rise to second-order interactions. Their effect on the calculated cross sections can be regarded as negligible, considering the accuracy of the results. The cluster quantum numbers (N, L, S, J), corresponding to the ^{112}Pd and ^{114}Cd transitions, were calculated based on shell orbitals, following the procedure described in Ref. [21]. In such conditions, the *relative* spectroscopic factors c^2s were chosen to be those that better describe the experimental excitation function for the reactions ^{110}Pd(^{18}O,^{14}C)^{114}Cd (2_1^+), ^{110}Pd(^{18}O,^{16}O)^{112}Pd ($2_1^+, 4_1^+$) (Figs. 4 and 5), and the quasielastic data (Fig. 6), near and below the barrier energies ($\langle E_{\rm lab}\rangle \leqslant 51.5$ MeV), according to the CC calculations. For the ^{110}Pd(^{18}O,^{16}O)^{112}Pd $0^+_{\rm gs}, 0^+_2, 2^+_2$, and ^{110}Pd(^{18}O,^{14}C)^{114}Cd $0^+_{\rm gs}, 0^+_2, 2^+_2, 4^+_2$ excitations, the corresponding spectroscopic factors (s.f.) were assumed to be identical to those of one- or two-phonon states that have been chosen as described above. The transfer s.f. that have been determined and used in the present work are listed in Table II. The real potential used in the exit channels of the transfer reactions discussed above were derived from the S Paulo potential model (1) using ground-state (gs) densities from systematics based on HFB calculations as described in Ref. [3]. Within such conditions, a large amount of extensive CC calculations have been performed to describe simultaneously the γ-particle coincidence measurements and quasielastic cross sections in the energy interval $42 \leqslant E_{\rm lab} \leqslant 58$ MeV. In the calculations, as mentioned above, only the β_N real potential deformation parameters were allowed to vary, and about 500 partial waves were necessary to be taken into account for convergence. In the case of γ-particle cross sections, due to the large beam energy loss through the target, the calculations have been performed in 10 ΔE steps of 0.285 MeV for each energy to obtain reliable average cross-section values. Uncertainties due to straggling effects in the determination of the average beam energy were also taken into account (dashed lines in Figs. 3, 4, and 5) and are more relevant for energies below the barrier. The overall description of the data (Figs. 3, 4, 5, and 6) is quite reasonable. Both the order of magnitude of the cross sections of the different

channels and the general tendencies are well reproduced by the calculations. We point out the good agreement between the full CC calculation results (solid lines) and the experimental data for energies $E_{\rm lab} \leqslant 1.15 V_B$, which is compatible with that from similar analyses for the ^{18}O+^{58}Ni [16]. For higher energies, as shown for the inelastic excitations (Fig. 3), the agreement is comparatively worse. In the ^{18}O+^{58}Ni case, it has been possible to describe the experimental data with the same good precision up to $E_{\rm lab} \approx 2V_B$. This is probably due to the different nuclear structure of the two target mass regions: in the nearly spherical ^{58}Ni only the one- and two-phonon states are available below $E^* = 2.5$ MeV, whereas for the transitional ^{110}Pd, with many other states in the same energy region, additional couplings should be taken into account as the bombarding energy increases. In the present CC data analysis, as mentioned before, no imaginary optical potential has been used in the surface region, indicating that other dynamical polarizations such as friction and deep inelastic collisions are higher-order effects as compared with those included in the present calculations. Some interesting features of the present CC calculations should be mentioned:

(i) The data obtained with the γ-particle coincidence method were essential for the CC calculation to define the $2n$ transfer spectroscopic factors at low energy and to characterize the region of "reasonable" β_N parameters, whereas the quasielastic data (with less sensitivity to the inelastic and transfer couplings) were fundamental for defining the main couplings to the elastic channel.

(ii) A high sensitivity to the bare potential of the CC data analysis was observed. Indeed, a variation of about 15% in the diffuseness parameter (a) of the equivalent WS shape bare potential strongly deteriorates the agreement with experimental data.

(iii) With the precision of the experimental data, particularly those from the γ-particle coincidence method, it was not possible to determine the potential deformation parameters β_N with high accuracy (see Table I). The sensitivity to the β_N parameters is enhanced for energies above the barrier. Even considering the uncertainties, they are relatively small as compared to the corresponding β_C values. This behavior is also observed in the ^{110}Pd (α, α') [13] data analysis and others [22] but has not been detected in the nearly spherical ^{58}Ni region, where $\beta_N \approx \beta_C$, as expected. In the present analysis, the agreement with the data sharply deteriorates for $\beta_N \approx \beta_C$ (see Fig. 3). However, as discussed in Ref. [23] (which is based on Satchler's theorem [24]), there are large ambiguities in the nuclear deformation parameters when they are extracted from optical potential or folding model analyses. The experimental nuclear multipole matrix elements, however, show much greater consistency when compared with their corresponding Coulomb matrix elements. This point remains to be investigated in future work.

(iv) The role played by the two-neutron transfer couplings is relatively small in comparison with the similar CC data analysis in the ^{58}Ni region. Probably, this effect is due to the pairing correlation that is somewhat deteriorated in the $A \approx 100$ transitional region, due to the proximity of the neutron and proton shell orbitals. This fact is also consistent with the relatively small s.f. values for the two-neutron transfer reactions ($\approx$0.1$-$0.2), in comparison with those in the Ni region.

(v) The significance of the α-transfer channel couplings in the full CC calculation was evidenced by the quasielastic results (Fig. 6). This behavior has not been detected in the Ni region.

(vi) Particularly for near- and below-barrier energies, the calculations predict a considerable importance of one-neutron transfer couplings in the CC calculation (Fig. 6).

(vii) Despite the appreciable β-deformation values for inelastic states and low excitation energy ($E^* < 1.0$ MeV), the full CC calculation is determined not only by inelastic couplings, as the transfer channel couplings also play an important role.

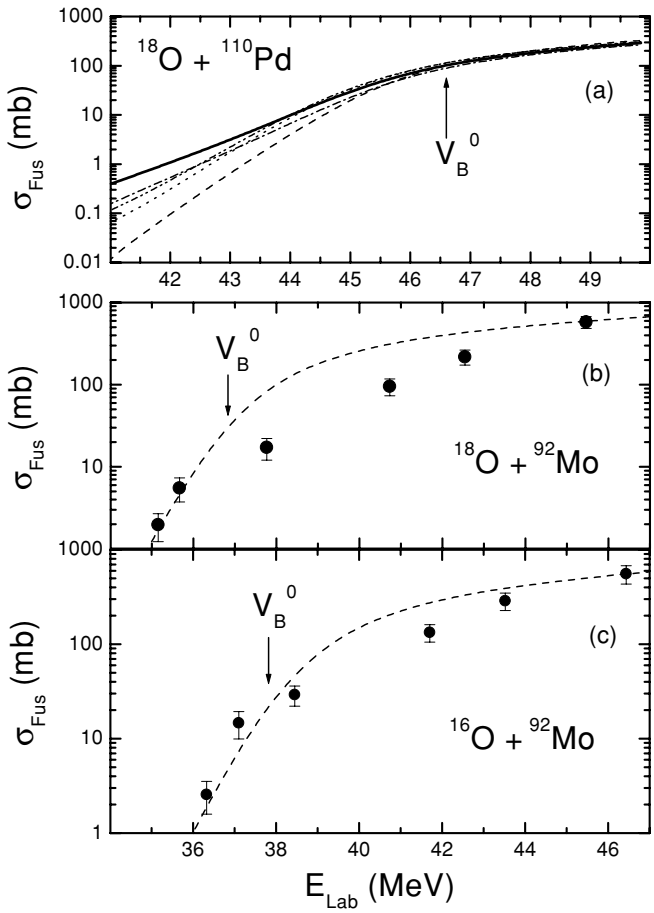

FIG. 7. (a) The fusion cross sections for the ^{18}O+^{110}Pd system as predicted from the present CC data analysis. (b) and (c) Experimental fusion cross sections obtained with γ-ray detection method (closed circles), for (a) ^{18}O+^{92}Mo and (b) ^{16}O+^{92}Mo [25]. The lines correspond to the CC calculation results considering: no-coupling (dash); inel only (dot); inel + $2n$ (dash-dot-dot); inel + $2n$ + α (dash-dot); and inel + $2n$ + α + $1n$ = full CC (solid).

IV. DISCUSSION ON FUSION HINDRANCE AND ENHANCEMENT IN THE ^{18}O+^{110}Pd SYSTEM

As a consequence of the CC quasielastic data analysis performed for the ^{18}O+^{110}Pd system, fusion cross sections can be predicted for this system (Fig. 7) in the energy interval $41 < E_{cm} < 50$ MeV. Unfortunately, there are no experimental data available to compare with the theoretical predictions. However, consistent with the present CC data analysis, the theoretical calculations predict a small contribution of the two neutron transfer couplings for near barrier energies. No fusion cross section hindrance with relation to the no-coupling (bare) results (see dashed line in the figure) is predicted, a completely different behavior when compared with that for the ^{18}O+^{58}Ni system, where the $2n$ transfer coupling gives rise to fusion hindrance for energies slightly above the barrier. The $1n$ and α couplings in the fusion channel are important particularly for near- and below-barrier energies. For above-barrier energies the fusion cross section is determined by the no-coupling results, with a very small contribution of the α-transfer coupling. The subbarrier enhancement relative to the bare results has an important contribution, as expected, from inelastic couplings, which is complemented by the transfer couplings. The enhancement, as shown in Fig. 7(a), is about 1–2 orders of magnitude greater in comparison with the bare results, in the low-energy region.

Figures 7(b) and 7(c) show experimental fusion cross sections for the nearly closed-shell systems ^{16,18}O+^{92}Mo [25], for comparison purposes. The theoretical no-coupling calculations for the fusion channel (dashed lines), using the parameter free São Paulo potential as the bare potential, are also shown in the figure. The experimental data points below the barrier are close to the theoretical bare results, considering the error bars, suggesting a small sub-barrier fusion enhancement. For the system with ^{18}O beam there in an indication of fusion hindrance slightly above the barrier as in the Ni region system.

V. SUMMARY AND CONCLUSIONS

In this work we present a realistic CC data analysis with the São Paulo potential as the bare interaction in the $A \approx 100$ transitional region. The experimental data obtained with a combination of the γ-particle coincidence method (low-lying excited states of the inelastic and transfer processes) and inclusive quasielastic cross sections (particle detection method) allows us to determine the relevant deformation parameters and transfer spectroscopic factors. Within these conditions, we performed a consistent CC description of the experimental data. Our results show a quite different role played by the channel couplings relative to a similar data analysis in the nearly spherical region (^{58}Ni). Our studies also show that more systematic experimental examples are necessary in the transitional and deformed regions, and there is room to improve the experimental methods used in the present work.

ACKNOWLEDGMENTS

We thank Dr. K. Ernst Rehm for his important collaboration in the proposal and in the γ-particle measurements of this work. This work was partially supported by the Fundação de Amparo à Pesquisa do Estado de São Paulo (FAPESP), Conselho Nacional de Desenvolvimento Científico e Tecnológico (CNPq), and Financiadora de Estudos e Projetos (FINEP).

[1] M. A. Candido Ribeiro, L. C. Chamon, D. Pereira, M. S. Hussein, and D. Galetti, Phys. Rev. Lett. **78**, 3270 (1997).
[2] L. C. Chamon, D. Pereira, M. S. Hussein, M. A. Candido Ribeiro, and D. Galetti, Phys. Rev. Lett. **79**, 5218 (1997).
[3] L. C. Chamon, B. V. Carlson, L. R. Gasques, D. Pereira, C. De Conti, M. A. G. Alvarez, M. S. Hussein, M. A. Candido Ribeiro, E. S. Rossi Jr., and C. P. Silva, Phys. Rev. C **66**, 014610 (2002).
[4] L. C. Chamon, D. Pereira, and M. S. Hussein, Phys. Rev. C **58**, 576 (1998).
[5] M. A. G. Alvarez, E. S. Rossi Jr., C. P. Silva, L. R. Gasques, L. C. Chamon, D. Pereira, M. N. Rao, B. V. Carlson, C. De Conti, R. M. Anjos, P. R. S. Gomes, J. Lubian, S. Kailas, A. Chatterjee, and P. Singh, Phys. Rev. C **65**, 014602 (2001).
[6] V. P. Likhachev, J. Mesa, J. D. T. Arruda-Neto, B. V. Carlson, W. R. Carvalho Jr., L. C. Chamon, A. Deppman, H. Dias, and M. S. Hussein, Nucl. Phys. **A713**, 24 (2003).
[7] L. R. Gasques, L. C. Chamon, D. Pereira, V. Guimarães, A. Lépine-Szily, M. A. G. Alvarez, E. S. Rossi Jr., C. P. Silva, B. V. Carlson, J. J. Kolata, L. Lamm, D. Peterson, P. Santi, S. Vincent, P. A. De Young, and G. Peasley, Phys. Rev. C **67**, 024602 (2003).
[8] L. R. Gasques, L. C. Chamon, D. Pereira, M. A. G. Alvarez, E. S. Rossi Jr., C. P. Silva, and B. V. Carlson, Phys. Rev. C **69**, 034603 (2004).
[9] P. R. S. Gomes, R. M. Anjos, C. Muri, J. Lubian, I. Padron, L. C. Chamon, R. Liguori Neto, N. Added, J. O. Fernández Niello, G. V. Martí, O. A. Capurro, A. J. Pacheco, J. E. Testoni, and D. Abriola, Phys. Rev. C **70**, 054605 (2004).
[10] J. J. S. Alves, P. R. S. Gomes, J. Lubian, L. C. Chamon, D. Pereira, R. M. Anjos, E. S. Rossi Jr., C. P. Silva, M. A. G. Alvarez, G. P. A. Nobre, and L. R. Gasques, Nucl. Phys. **A748**, 59 (2005).
[11] L. R. Gasques, A. V. Afasnajev, M. Beard, L. C. Chamon, P. Ring, and M. Wiescher, Nucl. Phys. **A758**, 134 (2005).
[12] L. R. Gasques, A. V. Afanasjev, E. F. Aguilera, M. Beard, L. C. Chamon, P. Ring, M. Wiescher, and D. G. Yakovlev, Phys. Rev. C **72**, 025806 (2005).
[13] V. Riech, R. Scherwinski, G. Lindström, E. Fretwurst, K. Gridnev, P. P. Zarubin, and R. Kolalis, Nucl. Phys. **A542**, 61 (1992).
[14] T. Czosnyka, D. Cline, and C. Y. Wu, Bull. Am. Phys. Soc. **28**, 745 (1983); GOSIA users manual, University of Rochester, UR-NSRL-305 (1991).
[15] E. S. Rossi Jr., D. Pereira, L. C. Chamon, C. P. Silva, M. A. G. Alvarez, L. R. Gasques, J. Lubian, B. V. Carlson, and C. De Conti, Nucl. Phys. **A707**, 325 (2002).
[16] D. Pereira, C. P. Silva, J. Lubian, E. S. Rossi Jr., and L. C. Chamon, Phys. Rev. C **73**, 014601 (2006).
[17] I. J. Thompson, Comput. Phys. Rep. **7**, 167 (1988).

[18] L. C. Chamon, G. P. A. Nobre, D. Pereira, E. S. Rossi Jr., C. P. Silva, L. R. Gasques, and B. V. Carlson, Phys. Rev. C **70**, 014604 (2004).
[19] J. Blachot, Nuclear Data Sheets **77**, 299 (1996).
[20] K. E. Rehm, W. Henning, J. R. Erskine, and D. G. Kovar, Phys. Rev. C **26**, 1010 (1982).
[21] G. R. Satchler, *Direct Nuclear Reactions* (Oxford University Press, New York, 1983).
[22] I. Y. Lee, J. X. Saladin, C. Baktash, J. E. Holden, and J. O'Brien, Phys. Rev. Lett. **33**, 383 (1974).
[23] R. S. Mackintosh, Nucl. Phys. **A266**, 379 (1976).
[24] G. R. Satchler, J. Math. Phys. **13**, 1118 (1972).
[25] M. Benjelloun, W. Galster, and J. Vervier, Nucl. Phys. **A560**, 715 (1993).